Nano Research 2016, 9(9): 2803–2810
DOI 10.1007/s12274-016-1169-8
Research Article
ISSN 1998-0124
CN 11-5974/O4

Impurity-induced formation of bilayered graphene on copper by chemical vapor deposition

Jun Li[1,2], Jianing Zhuang[3], Chengmin Shen[1,4] (✉), Yuan Tian[1], Yande Que[1,2], Ruisong Ma[1,2], Jinbo Pan[1,2], Yanfang Zhang[1,2], Yeliang Wang[1,4], Shixuan Du[1,4], Feng Ding[3] (✉), and Hong-Jun Gao[1,4] (✉)

[1] *Beijing National Laboratory for Condensed Matter Physics, Institute of Physics, Chinese Academy of Sciences, Beijing 100190, China*
[2] *University of Chinese Academy of Sciences, Beijing 100049, China*
[3] *Institute of Textiles and Clothing, Hong Kong Polytechnic University, Kowloon, Hong Kong, China*
[4] *Beijing Key Laboratory for Nanomaterials and Nanodevices, Beijing 100190, China*

Received: 7 April 2016
Accepted: 2 June 2016

KEYWORDS
graphene,
chemical vapor deposition (CVD),
bilayer,
growth mechanism

ABSTRACT

High-quality single-layered and bilayered graphene (SLG and BLG) was synthesized on copper foil surfaces by controllable chemical vapor deposition (CVD). Impurity nanoparticles formed on the copper foil surface by high-temperature annealing were found to play a crucial role in the growth of BLG. Analysis of energy-dispersive spectrometry (EDS) data indicated that these nanoparticles consisted of silicon and aluminum. According to the inverted wedding cake model, these nanoparticles served as nucleation centers for BLG growth and the free space between a nanoparticle and graphene served as the center of C injection for the continuous growth of the adlayer beneath the top layer. By combining phase-field theory simulations, we confirmed the mechanism of BLG growth and revealed more details about it in comparison with SLG growth. For the first time, this study led to a complete understanding of the BLG growth mechanism from nucleation to continuous growth in the CVD process, and it has opened a door to the thickness-controllable synthesis of graphene.

1 Introduction

Graphene is one of the most promising materials since the fabrication of complementary metal–oxide–semiconductor (CMOS) structures because of its unique properties [1, 2]. For some applications in electronics and optoelectronics, particularly in logic and switching circuits, a bandgap is required. Therefore, much effort has been made to develop a proper bandgap-opening strategy, including preparation of nanoribbons [3], stress-induction engineering [4], chemical element doping [5], and tuning the number of graphene layers [6]. Among these strategies, bilayered graphene (BLG) can be tuned to become a 250-meV bandgap semiconductor by applying a perpendicular electric field without excessively disrupting the carrier mobility;

Address correspondence to Chengmin Shen, cmshen@iphy.ac.cn; Feng Ding, feng.ding@polyu.edu.hk; Hong-Jun Gao, hjgao@iphy.ac.cn

this strategy has attracted much research interest [7]. McCann calculated the band structure of BLG by using the tight-binding model and opened a gap between the conduction band and valence band [8]. Wang et al. directly observed a widely tunable bandgap in dual-gate BLG field-effect transistors (FETs) [6]. Avouris et al. reported on/off current ratios of about 100 and 2,000 at room temperature and 20 K, respectively, in dual-gate BLG FETs [9]. Therefore, BLG seems very promising for future generations of high-performance electronic and photonic devices.

However, it is still very challenging to grow large-sized, high-quality BLG under experimental conditions. Chemical vapor deposition (CVD) has been widely used in the preparation of large-scale graphene on transition-metal substrates. For example, wafer-scale homogeneous BLG films have been synthesized on Cu foils under tunable conditions [10]. Bernal-stacked BLG films on Cu foils have been produced using two-step epitaxial growth via CVD. In addition, AB-stacked BLG films have been synthesized on Cu–Ni alloy foils [11]. Although the growth of BLG has attracted much research interest, the growth mechanism of BLG remains unclear. Two different mechanisms have been proposed for BLG growth—the wedding cake model, in which the adlayer grows above the first layer; the inverted wedding cake model, in which the adlayer grows beneath the first layer [12]. For metal catalysts with higher carbon solubility (such as Ir, Ru, Ni), the inverted wedding cake model is a reasonable mechanism because of the precipitation of carbon from the catalyst to the space beneath the first graphene layer. However, it is not a realistic explanation of BLG growth on a Cu substrate because of the very low solubility of carbon in copper and the self-limited growth. Kong et al. measured the stacking order of BLG grown on Cu by isotope labeling and showed that the inverted wedding cake model was still valid [13]. Subsequently, Cai et al. found that the adlayer was formed at the same nucleation points and its growth was terminated simultaneously with that of the first layer [14]. Banerjee's group observed that the purity of a Cu surface could enhance its catalytic capability, leading to methane decomposition to form a high concentration of carbon atoms [15]. A key problem in understanding BLG growth is determining the origin of carbon atoms that are required to form the adlayer graphene beneath the top layer during isothermal CVD growth. So far, there has been no clear answer.

Here, we present an unambiguous answer to the above question—the formation of the graphene adlayer beneath the top layer is closely associated with impurity particles formed during annealing of the Cu foil; its nucleation begins with the impurity nanoparticles, and its growth is supported by the diffusion of feedstock through the gaps between these nanoparticles and the surrounding graphene to the space beneath the graphene top layer. In our study, we found that the impurity particles that formed on the Cu foil surface during high-temperature annealing dramatically changed the number of graphene layers. Therefore, mostly single-layered graphene (SLG) formed on Cu foil in the low-temperature CVD experiments and BLG formed at high temperature.

2 Experimental

2.1 Synthesis of graphene

Graphene was prepared on commercially available 250-μm-thick Cu foils (Sigma Aldrich 349178, 99.98% purity) in a quartz-tube furnace, as shown in Fig. S1 in the Electronic Supplementary Material (ESM). A typical graphene growth process is shown schematically in Fig. S2 in the ESM. To remove the absorbents and contaminants on the copper surface, as well as to increase the copper grain size, the foils were first cleaned by sonication for 10 min each in acetone and ethanol. They were then immersed in hydrochloric acid (about 15% HCl) for 1 min, followed by repeatedly rinsing with deionized (DI) water and drying under a nitrogen gas flow. Later, the copper foil was annealed at 1,060 °C and held for 30 min under a H_2–Ar mixed-gas flow at 200 standard cubic centimeters per minute (sccm) at standard temperature and pressure (H_2/Ar volume ratio of 20:180 sccm) and a pressure of 1.0×10^4 Pa. Subsequently, 0.5 sccm of methane (CH_4) was introduced to the furnace for graphene growth for a fixed duration. In order to obtain graphene islands, the growth time was controlled to be less than 60 s. When the growth time exceeded 3 min, a graphene

film appeared. Finally, the furnace was naturally cooled to room temperature under a pressure of 1.0×10^4 Pa and H_2–Ar gas flow at 200 sccm.

2.2 Characterization

The morphology of graphene was obtained by scanning electron microscopy (SEM; RAITH150, Raith and JBX-6300FS, JEOL), and elemental analysis of the copper foil surface was carried out by energy-dispersive spectrometry (EDS) (Model XL-SFEG SEM with a Schottky field-emission gun (SFEG) as the electron source and a built-in EDS system, FEI Crop, Hillsboro, OR). Raman spectrometry was used to evaluate the quality and number of layers of graphene (LabRAM HR-Evolution, Horiba Jobin Yvon), with a 532-nm laser as the excitation light, an estimated laser spot size of 1 μm, and laser power of 5 mW. The surface structure of graphene was examined using a scanning probe microscope (SPM; Multimode Nanoscope, Veeco).

3 Results and discussion

Figure 1(a) shows an SEM image of the copper foil surface (before graphene growth) after annealing at 1,060 ℃ under a mixed flow of 10% H_2 (by volume) and 90% Ar at 200 sccm for 30 min. Many small white nanoparticles (white dots in the image) appeared randomly on the surface of the copper foil, and they were about 100 nm to several hundred nanometers in diameter. Our analysis of the EDS results indicated that the white nanoparticles consisted of silicon and aluminum (Fig. 1(b)) owing to contaminants in the bulk of the copper foil migrating to the interior surface of the quartz tube during high-temperature annealing. Similar results were previously reported in Refs. [16–19]. In particular, Wang et al. observed by *in situ* SEM that this type of white nanoparticles began to appear when the annealing temperature was above 800 ℃, and these nanoparticles became mobile and started drifting across the surface in more or less random directions when the temperature exceeded 850 ℃ [16]. The high-resolution (HR)-SEM image in Fig. 1(d) shows that the white nanoparticles actually had a fractal structure. Despite the large quantity of nanoparticles on the copper surface, hexagonal SLG could still be prepared with a growth time of 1 min at 1,060 ℃ under a flow of CH_4 at 0.5 sccm and a mixed flow of 10% H_2 and 90% Ar at 200 sccm (Fig. 1(c)). We can see from Fig. 1(c) that most of the white dots were no longer randomly arranged, and they were aligned uniformly along the graphene domain edge. At high temperature (the temperature of graphene growth was 1,060 ℃), the white dots shifted constantly and there were many dangling bonds around the graphene edges, both of which resulted in alignment of the white dots after graphene growth. Figures 1(e) and 1(f) show a single graphene island and its edge. Compared with the structure of a freestanding white dot in Fig. 1(d), it can be easily seen that only half of each nanoparticle was around a graphene island. This means that the other half of each particle was filled beneath the copper surface near the graphene edge because the copper atoms and nanoparticles were all continually shifting at

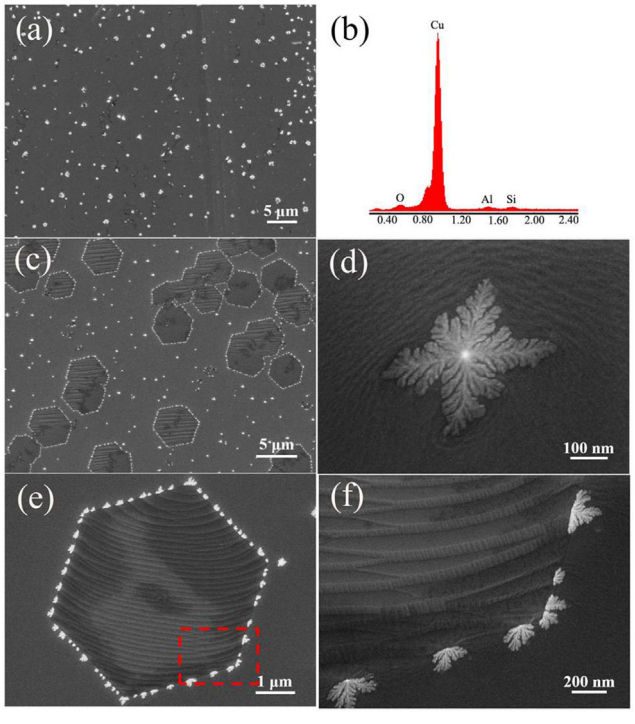

Figure 1 (a) SEM image of Cu surface after annealing at 1,060 ℃ (before graphene growth). (b) Typical EDS result of a white particle from the Cu surface shown in (a) (the spectrum was recorded at an acceleration voltage of 15 keV). (c) SEM image of graphene islands after 1 min of growth. (d) High-resolution SEM image of a free-standing white particle. SEM images of (e) a hexagonal graphene island and (f) its edge.

temperatures below 1,060 ℃. In addition, copper terraces can be clearly seen, and they resulted from the protection of graphene on the copper surface against oxidization. In contrast, if the copper foil was not covered by a graphene film, a thin layer of copper oxide would have developed after about three days and the copper surface would have grown flat, as shown in Fig. S3 in the ESM. Thus, the presence of copper terraces is one of the criteria for graphene growth on a copper surface.

In order to understand the growth mechanism of graphene in the presence of the white nanoparticles, atomic force microscopy (AFM) was used to characterize the morphology of graphene. Figure 2(a) shows an AFM image of graphene islands and graphene edges. The islands and edges are marked by white dashed lines in Fig. 2(a), and it can be clearly seen that there was a hole around each free-standing particle (marked by a red dashed circle) because the dots of white nanoparticles and copper were immiscible at high temperature. In addition, there was an obvious

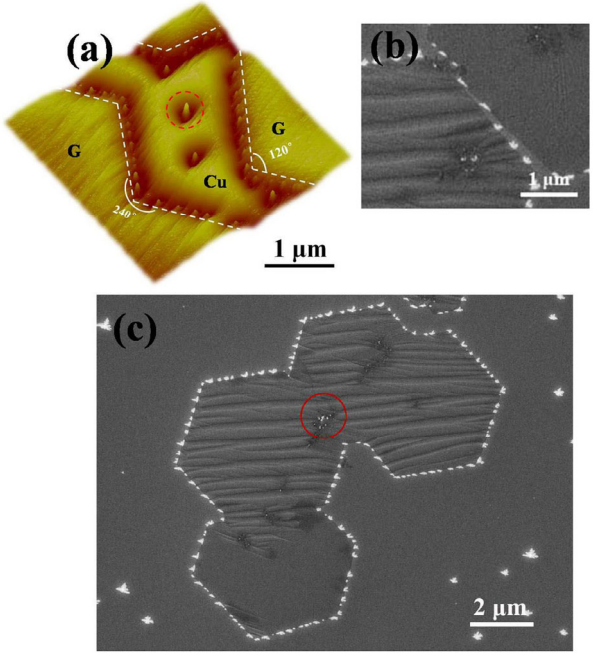

Figure 2 (a) Three-dimensional AFM image of graphene domains on a copper surface; the white lines delineate the domain edges. A free-standing particle is marked by a red dashed circle, which corresponds to the white dot in Fig. 1(d). "G" stands for graphene and "Cu" marks the bare Cu surface on which there was no graphene growth. (b) SEM image of two coalescing graphene islands. (c) SEM image of four coalescing graphene islands.

channel along each graphene edge except for the white dots. The depth of these channels was about 200 nm, and they may have arisen from the mobility of liquid copper and the white dots at high temperature. When graphene grew on the surface of the Cu foil, the graphene pushed the white dots to the edges, resulting in channels between copper and the white dots after the reaction stopped. As the reaction time was increased, the angle of 240° represents the point where two graphene domains coalesced, but no white dots were visible. Figure 2(b) shows two graphene domains merging together, with the white dots buried in the channel along the graphene edges. Figure 2(c) shows four coalescing graphene islands without any grain boundaries because they had the same orientations. Only a small quantity of white particles were still exposed in the graphene, as shown by the red circle in Fig. 2(c), and this kind of particles played an important role in the growth of the next layer of graphene.

As the growth duration was increased, graphene domains continued to coalesce, forming a graphene film when the growth duration exceeded 3 min, as shown in Fig. 3(a). Some overlapping wrinkles can be seen (marked by red arrows), and they were caused by the difference between the coefficients of thermal expansion of graphene and the copper substrate. As mentioned earlier, another hexagonal graphene layer appeared around each white particle. Figure 3(b) shows a typical adlayer region, and the edge of the adlayer is marked by red dotted lines. We can see that the shape of the adlayer was still hexagonal, but the angles of the domains were not as sharp as those in the islands of SLG. Figure 3(c) shows typical Raman spectra of graphene films that were recorded far from the white particles (SLG) or near a white particle (BLG). The D peak, which is due to disorder and typically observed at ~1,350 cm^{-1}, is absent in the SLG Raman spectrum, indicating a high degree of crystallinity in the monolayer. The G peak, which is due to the doubly degenerate zone center E_{2g} mode, appears at ~1,585 cm^{-1} in both SLG and BLG spectra [20]. The 2D peak appears at ~2,693 cm^{-1} and has a line width (full width at half maximum or FWHM) of ~25 cm^{-1}. In the BLG region, however, the 2D peak position at ~2,702 cm^{-1} (FWHM: 50 cm^{-1}) is blue-shifted compared to that in the SLG

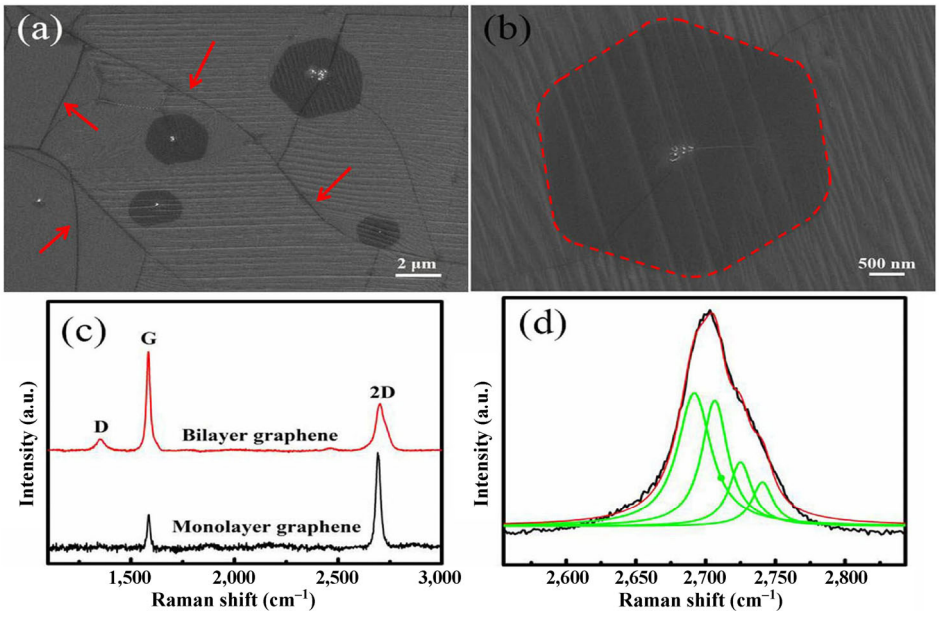

Figure 3 SEM images and Raman spectra of single-layered and bilayered graphene (SLG and BLG, respectively). Note that the baselines of the spectra shown in (c) and (d) had been corrected to account for the broad luminescence background from the Cu substrate.

region, and it can be fitted with four Lorentzian peaks, as shown in Fig. 3(d). Moreover, an obvious D peak can be seen at ~1,350 cm^{-1} in the BLG spectrum, and it corresponds to the white particle at the center of the bilayer region. By analyzing many Raman scattering results of CVD-grown graphene on copper substrates, we have learnt that there must be a white particle at the center of each BLG domain. The same results have also been reported for many studies of BLG grown on copper [12, 21, 22]. Occasionally, regions of trilayered graphene also appear around impurities (Fig. S4 in the ESM). Therefore, the white particles played an essential role in growth of the graphene adlayer.

The difference between the graphene domain shapes during SLG and adlayer growth implies a difference in the growth processes. For the SLG growth on a copper surface (Fig. 4(a)), the growth of a domain would gradually absorb C precursors around it; as a consequence, a depletion zone would be formed around the domain [16]. With the formation of the depletion zone, a domain edge that was far from the center could be attached to more carbon precursors and its growth could become faster than that of edges closer to the precursor. This would eventually result in fractal-shaped graphene domains or regular hexagonal domains with sharp edges [23]. If the adlayer grew on top of the first layer (Fig. 4(b)), the carbon supply should be very similar to that for the SLG growth, which would negate the need to form hexagonal domains with rounded corners. If the adlayer grew beneath a complete first layer, the carbon supply would reach the underlying area only through diffusion from the area near the impurity particles (Fig. 4(c)). Consequently, the area near the center of the domain would have a high precursor concentration, and the area around the corner, which was far from the center, would have lower carbon concentration. This is in sharp contrast to the growth of SLG domains on a Cu surface. Under such condition, it was possible for growth of the edge near a vertex of the hexagon to be slower, and the hexagonal graphene domains would eventually evolve into a shape with rounded corners as a result.

To verify the above speculation, we performed serious phase-field simulations of graphene growth with different boundary conditions (see the ESM for details), as shown by the results in Figs. 4(a) and 4(c). For the growth of the SLG domain on a Cu surface, the carbon-precursor flux reached the entire area of the substrate that was not covered by graphene (Fig. 4(a)). On the other hand, for the growth of the adlayer beneath the top layer, the carbon precursor

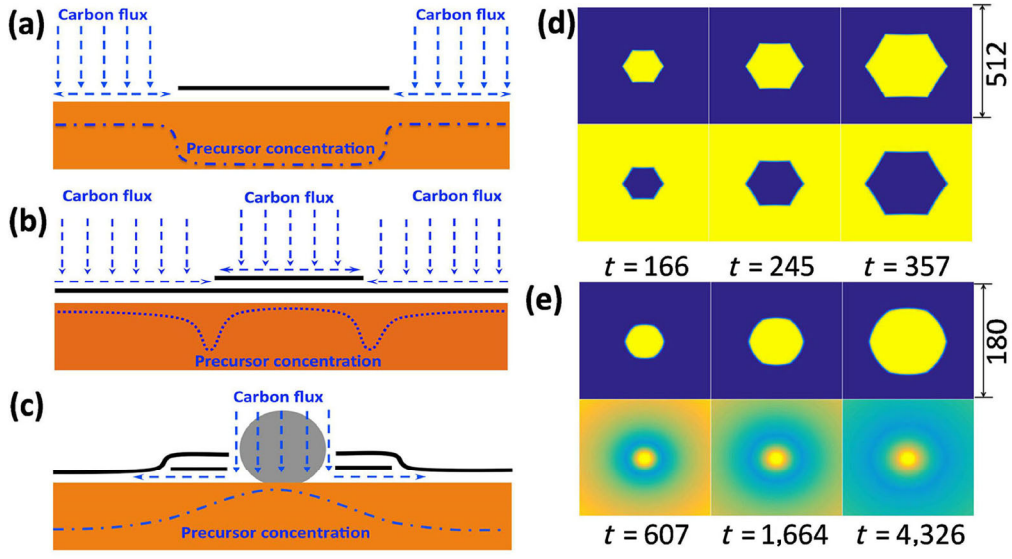

Figure 4 (a) Illustration of SLG growth on Cu. (b) Illustration of growth of the second layer above the first graphene layer. (c) Illustration of growth of the second layer under the first graphene layer, with the help of an impurity particle. (d) Phase-field simulation of growth of the first graphene layer, together with the concentration field, at simulation time of 166, 245, and 357. (e) Phase-field simulation of growth of the second graphene layer corresponding to (c), together with the concentration field, at simulation time of 607, 1,664, and 4,326. Details of the phase-field simulations are presented in the ESM.

reached the substrate through a very small area around an impurity particle (Fig. 4(c)). Figure 4(d) shows the simulated growth process of SLG domains on the Cu surface; a sharp-edged hexagon and a depletion zone around the domain are clearly visible in the concentration map. Figure 4(e) presents the graphene domain obtained when the C precursor reached the substrate from only the central area. The domain always exhibited a shape with rounded corners, and the concentration map clearly shows a high concentration peak near the center and a gradual reduction in concentration from the center to the surrounding area. It is important to note that the SLG growth was more than one order of magnitude faster than the adlayer growth owing to the large carbon flux around the domain on the catalyst surface.

The theoretical results in Fig. 4 clearly indicate that the adlayer grew beneath the first layer and the C supply originated from the defective area near the impurity particle. Therefore, the dual roles of the impurity particle in both the nucleation of graphene adlayer domain and the C precursor supply are validated.

In order to prove the proposed mechanism of BLG growth, we tried to eliminate the effect of the white particles on graphene growth. The copper substrates were etched by argon in a reactive-ion etching (RIE) system (O_2 flow: 100 sccm; pressure: 100 mTorr; power: 100 W; duration: 1 min) before graphene growth. In addition, the annealing temperature and growth temperature were decreased to 1,000 ˚C, while the other conditions remained unchanged. After graphene growth, no white particles were observed on the copper substrates, as shown in Fig. 5. Either graphene islands (Fig. 5(a)) or graphene film (Fig. 5(b)) could be obtained by controlling the growth time. Figure 5(c) shows a typical Raman spectrum collected from a graphene island (Fig. 5(a)), which is similar to that of the graphene film (Fig. 5(b)). The G peak appears at ~1,592 cm^{-1}, and the 2D peak appears at ~2,697 cm^{-1}, with a FWHM of ~28 cm^{-1}; these are typical characteristics of monolayered graphene. In other words, only single-layered graphene domains or a single-layered graphene film was prepared on the copper foil with no impurities. Moreover, at each of the graphene edges, there was no channel. Since channels are known to always appear at the graphene edge with impurities (Fig. 5(d)), their absence confirms the absence of impurities.

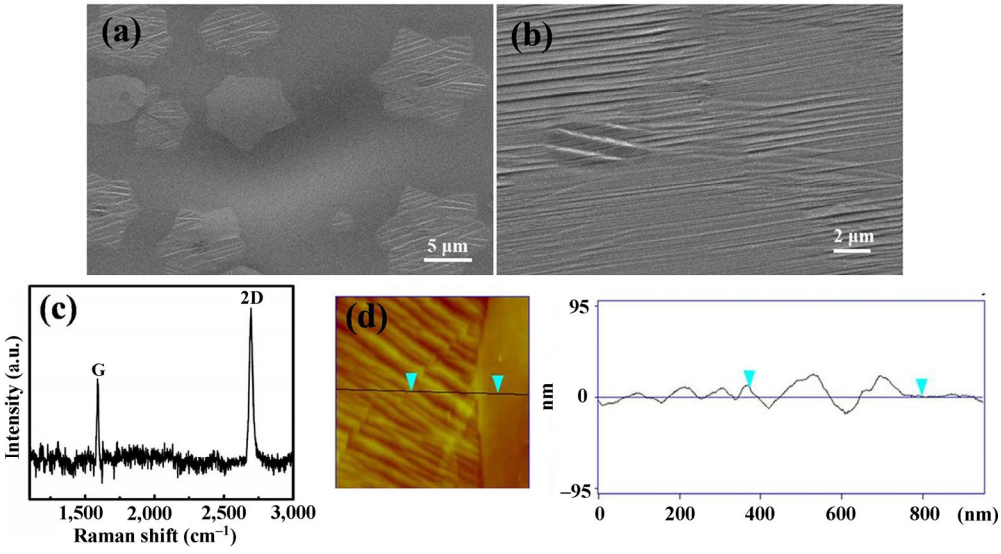

Figure 5 (a) and (b) SEM images of graphene islands and graphene film synthesized on copper substrates with no white particles. In (b), copper terraces can be seen clearly, which means the copper surface was completely covered by graphene and protected against oxidization. (c) Typical Raman spectrum collected from a graphene island in (a). (d) AFM image of a graphene domain edge; the left side with a copper terrace was covered by graphene.

4 Conclusions

This work demonstrates that when graphene was grown by CVD on the surface of clean copper (without impurities), only monolayered graphene islands or a graphene film was obtained. In other words, the "self-limited growth" process is a fully accurate description of graphene growth on a clean copper surface. For graphene growth on a copper surface with some impurities, however, bilayered or even few-layered graphene may appear around each impurity particle owing to impurity-assisted nucleation and injection of feedstock from the impurities. This study clearly demonstrated the process of BLG growth from the nucleation stage to the feedstock supply, as well as the effect on graphene domain formation. We have further proved that by carefully designing the catalyst, such as introducing or eliminating impurities, controllable synthesis of graphene could be attained. This strategy is expected to play an important role in future electronic applications.

Acknowledgements

This work was supported by the National Basic Research Program of China (No. 2013CBA01603), the National Natural Science Foundation of China (No. 61335006), and Chinese Academy of Sciences (Nos. 1731300500015 and XDB07030100).

Electronic Supplementary Material: Supplementary material (further details of the experimental procedures, STM measurements, SEM images, and phase field simulation) is available in the online version of this article at http://dx.doi.org/10.1007/s12274-016-1169-8.

References

[1] Geim, A. K.; Novoselov, K. S. The rise of graphene. *Nat. Mater.* **2007**, *6*, 183–191.

[2] Avouris, P.; Chen, Z. H.; Perebeinos, V. Carbon-based electronics. *Nat. Nanotechnol.* **2007**, *2*, 605–615.

[3] Han, M. Y.; Özyilmaz, B.; Zhang, Y. B.; Kim, P. Energy band-gap engineering of graphene nanoribbons. *Phys. Rev. Lett.* **2007**, *98*, 206805.

[4] Guinea, F.; Katsnelson, M. I.; Geim, A. K. Energy gaps and a zero-field quantum Hall effect in graphene by strain engineering. *Nat. Phys.* **2010**, **6**, 30–33.

[5] Wei, D. C.; Liu, Y. Q.; Wang, Y.; Zhang, H. L.; Huang, L. P.; Yu, G. Synthesis of N-doped graphene by chemical vapor deposition and its electrical properties. *Nano Lett.* **2009**, *9*, 1752–1758.

[6] Zhang, Y. B.; Tang, T.-T.; Girit, C.; Hao, Z.; Martin, M. C.; Zettl, A.; Crommie, M. F.; Shen, Y. R.; Wang, F. Direct observation of a widely tunable bandgap in bilayer graphene. *Nature* **2009**, *459*, 820–823.

[7] Castro, E. V.; Novoselov, K. S.; Morozov, S. V.; Peres, N. M. R.; Lopes dos Santos, J. M. B.; Nilsson, J.; Guinea, F.; Geim, A. K.; Castro Neto, A. H. Biased bilayer graphene: Semiconductor with a gap tunable by the electric field effect. *Phys. Rev. Lett.* **2007**, *99*, 216802.

[8] McCann, E. Asymmetry gap in the electronic band structure of bilayer graphene. *Phys. Rev. B* **2006**, *74*, 161403.

[9] Xia, F. N.; Farmer, D. B.; Lin, Y.-M.; Avouris, P. Graphene field-effect transistors with high on/off current ratio and large transport band gap at room temperature. *Nano Lett.* **2010**, *10*, 715–718.

[10] Lee, S.; Lee, K.; Zhong, Z. H. Wafer scale homogeneous bilayer graphene films by chemical vapor deposition. *Nano Lett.* **2010**, *10*, 4702–4707.

[11] Wu, Y. P.; Chou, H.; Ji, H. X.; Wu, Q. Z.; Chen, S. S.; Jiang, W.; Hao, Y. F.; Kang, J. Y.; Ren, Y. J.; Piner, R. D. et al. Growth mechanism and controlled synthesis of AB-stacked bilayer graphene on Cu–Ni alloy foils. *ACS Nano* **2012**, *6*, 7731–7738.

[12] Nie, S.; Wu, W.; Xing, S. R.; Yu, Q. K.; Bao, J. M.; Pei, S.-S.; McCarty, K. F. Growth from below: Bilayer graphene on copper by chemical vapor deposition. *New J. Phys.* **2012**, *14*, 093028.

[13] Fang, W. J.; Hsu, A. L.; Caudillo, R.; Song, Y.; Birdwell, A. G.; Zakar, E.; Kalbac, M.; Dubey, M.; Palacios, T.; Dresselhaus, M. S. et al. Rapid identification of stacking orientation in isotopically labeled chemical-vapor grown bilayer graphene by Raman spectroscopy. *Nano Lett.* **2013**, *13*, 1541–1548.

[14] Li, Q. Y.; Chou, H.; Zhong, J.-H.; Liu, J.-Y.; Dolocan, A.; Zhang, J. Y.; Zhou, Y. H.; Ruoff, R. S.; Chen, S. S.; Cai, W. W. Growth of adlayer graphene on Cu studied by carbon isotope labeling. *Nano Lett.* **2013**, *13*, 486–490.

[15] Liu, W.; Li, H.; Xu, C.; Khatami, Y.; Banerjee, K. Synthesis of high-quality monolayer and bilayer graphene on copper using chemical vapor deposition. *Carbon* **2011**, *49*, 4122–4130.

[16] Wang, Z.-J.; Weinberg, G.; Zhang, Q.; Lunkenbein, T.; Klein-Hoffmann, A.; Kurnatowska, M.; Plodinec, M.; Li, Q.; Chi, L. F.; Schloegl, R. et al. Direct observation of graphene growth and associated copper substrate dynamics by *in situ* scanning electron microscopy. *ACS Nano* **2015**, *9*, 1506–1519.

[17] Vlassiouk, I.; Regmi, M.; Fulvio, P. F.; Dai, S.; Datskos, P.; Eres, G.; Smirnov, S. Role of hydrogen in chemical vapor deposition growth of large single-crystal graphene. *ACS Nano* **2011**, *5*, 6069–6076.

[18] Zhang, Y.; Zhang, L. Y.; Kim, P.; Ge, M. Y.; Li, Z.; Zhou, C. W. Vapor trapping growth of single-crystalline graphene flowers: Synthesis, morphology, and electronic properties. *Nano Lett.* **2012**, *12*, 2810–2816.

[19] Wood, J. D.; Schmucker, S. W.; Lyons, A. S.; Pop, E.; Lyding, J. W. Effects of polycrystalline Cu substrate on graphene growth by chemical vapor deposition. *Nano Lett.* **2011**, *11*, 4547–4554.

[20] Ferrari, A. C.; Meyer, J. C.; Scardaci, V.; Casiraghi, C.; Lazzeri, M.; Mauri, F.; Piscanec, S.; Jiang, D.; Novoselov, K. S.; Roth, S. et al. Raman spectrum of graphene and graphene layers. *Phys. Rev. Lett.* **2006**, *97*, 187401.

[21] Wu, B.; Geng, D. C.; Guo, Y. L.; Huang, L. P.; Xue, Y. Z.; Zheng, J.; Chen, J. Y.; Yu, G.; Liu, Y. Q.; Jiang, L. et al. Equiangular hexagon-shape-controlled synthesis of graphene on copper surface. *Adv. Mater.* **2011**, *23*, 3522–3525.

[22] Yang, F.; Liu, Y. Q.; Wu, W.; Chen, W.; Gao, L.; Sun, J. A facile method to observe graphene growth on copper foil. *Nanotechnology* **2012**, *23*, 475705.

[23] Shu, H. B.; Chen, X. S.; Ding, F. The edge termination controlled kinetics in graphene chemical vapor deposition growth. *Chem. Sci.* **2014**, *5*, 4639–4645.